SANDIA REPORT

SAND2020-9592
Printed September 16, 2020

Sandia National Laboratories

Characterization and Sampling of Ultralow Permeability Geomaterials using Electrokinetics: LDRD Final Report (209234)

Kristopher L. Kuhlman, Melissa M. Mills, Pikee Priya, Narayana Aluru

Prepared by
Sandia National Laboratories
Albuquerque, New Mexico 87185
Livermore, California 94550

Issued by Sandia National Laboratories, operated for the United States Department of Energy by National Technology & Engineering Solutions of Sandia, LLC.

Available to DOE and DOE contractors from

U.S. Department of Energy
Office of Scientific and Technical Information
P.O. Box 62
Oak Ridge, TN 37831

Telephone: (865) 576-8401
Facsimile: (865) 576-5728
E-Mail: reports@osti.gov
Online ordering: http://www.osti.gov/scitech

Available to the public from

U.S. Department of Commerce
National Technical Information Service
5301 Shawnee Road
Alexandria, VA 22312

Telephone: (800) 553-6847
Facsimile: (703) 605-6900
E-Mail: orders@ntis.gov
Online order: https://classic.ntis.gov/help/order-methods

ABSTRACT

This final report on Laboratory Directed Research and Development (LDRD) project 209234 presents background material for electrokinetics at the pore and porous media scales. We present some theoretical developments related to uncoupling electrokinetic flow solutions, from a manuscript recently accepted into *Mathematical Geosciences* for publication. We present a summary of two pore-scale modeling efforts undertaken as part of the academic alliance with University of Illinois, resulting in one already submitted journal publication to *Transport in Porous Media* and another in preparation for submission to a journal. We finally show the laboratory apparatus built in Laboratory B59 in Building 823 and discuss some of the issues that occurred with it.

ACKNOWLEDGEMENT

Thanks to Erik Webb and Tracy Woolever from the Earth Science Research Foundation for funding the project. Thanks to Yifeng Wang and Pat Brady for encouragement and help with proposals and ideas. Thanks to Joseph Mohagheghi for help with 3D printing on an early iteration of the 823 laboratory device. Thanks to Bwalya Malama (Cal Poly San Luis Obispo), who collaborated on the Mathematical Geosciences paper and motivated this work in electrokinetics.

The Laboratory Directed Research and Development (LDRD) Academic Alliance with postdoc Pikee Priya and professor Narayana Aluru from the Beckman Institute at the University of Illinois at Urbana-Champaign (UIUC) has been fruitful and a learning experience for everyone involved. Thanks to Tom Corbet for assistance related to the academic alliance at Illinois.

The authors thank Matt Paul for technically reviewing the compiled SAND report.

CONTENTS

NOMENCLATURE

Abbreviation	Definition
BC	boundary conditions
DOE	Department of Energy
EDL	electric double layer
EO	electroosmosis
LDRD	Laboratory-Directed Research & Development
SP	streaming potential

1. INTRODUCTION

While many geophysical exploration methods are sensitive to the presence of water or solutes (e.g., electrical resistivity [59], seismic [37], or induced polarization [4]), the coupling between hydrology and geophysics is especially explicit and direct in electrokinetics [65, 64]. Direct causality exists between processes of water flow and electric potentials for streaming potentials and electrokinetics. Streaming potentials are caused by the movement of water through a porous medium and electroosmosis is the movement water in low-permeability porous media due to applied electric fields. Electrokinetics occur when electrolytes (e.g., water and ions) flow through a porous medium with a surface charge (e.g., quartz sand grains) [60, 16]. Streaming potentials arise from the movement of water under an imposed pressure gradient, dragging ions with the water, creating a streaming current. Electroosmotic pressure arises from the movement of ions under an imposed electric field, dragging the water with the ions, creating an electroosmotic flux.

Streaming potentials are a pore-scale phenomena that create useful effects at the laboratory and field scales to characterize water movement using passive (i.e., self-potential without an applied current) voltage observations [65, 62]. Field-scale streaming potentials have been used to derive material properties from field-scale pumping tests experiments [63, 50, 49, 48, 70]. Electroosmosis is utilized widely in microfluidics [40] and at the pore scale [21, 35] to move fluids through small pores. At the laboratory and field scale electroosmosis has been used to consolidate soft clays [9, 10, 45, 6] or mobilize contaminants [17, 2, 69, 1, 73, 14]. Seismoelectric applications consider the electrokinetic response (i.e., both streaming potential and electroosmosis) of a porous formation to seismic waves [60, 36, 64, 56].

The pore-scale electrokinetic problem involves solving the Navier-Stokes equation for fluid flow, the Nernst-Planck equations for ion transport, and the Poisson equation for excess charge redistribution. At this scale, the pore walls or grain boundaries are individually resolved (i.e., $\approx \mu$m). These small-scale problems are simulated to better understand and predict the physical processes at the porous media or field-relevant scale. At the porous media scale it can be straightforward to propose solvable governing equations, but difficult to physically justify these relationships (i.e., upscale or derive relationships that include all the physics from the smaller scale). At the porous media scale individual grains or fractures are not resolved (i.e., $\gg$ cm) and the equations rely on the existence of a representative elementary volume [25]. At this larger scale we use the groundwater flow (diffusion) equation and the Laplace equation for electrostatic excess charge redistribution. The equations at the porous media scale have terms with assumed or inferred coefficients. The academic alliance part of this LDRD involves simulating the problem at pore and macro scales with the hopes to improve the understanding of the relation between the processes.

Solid surfaces at the pore scale have fixed charge for a given solution composition (e.g., pH); ions in solutions within fractures and pores arrange themselves to balance out the surface charge (Figure 1-1). The more ordered region of ions near the surface is the bound part of the double layer (i.e., Stern layer), while a less bound region of ions is the diffuse part of the double layer (i.e., beyond the slipping plane). In both regions, most water molecules are free to move [38]

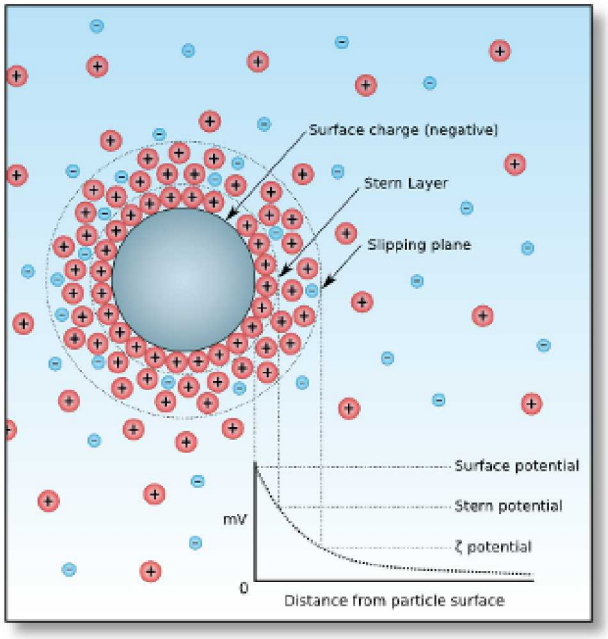

Figure 1-1. Ion distribution around a charged solid (Wikipedia)

(except the layer of water molecules immediately adjacent to the surface). With no fluid flow the steady-state double layer of counterions (i.e., cations in the case of negatively charged silica surfaces at typical pH) around a charged surface is given solely by the electrostatic arrangement of excess charges in the liquid around the charged solid surface (balance of Nernst-Planck and Poisson equations). This static distribution of excess charge – only influenced by electrostatic forces – will follow the Boltzmann distribution.

The porous media scale problem can be developed by scaling it up from the pore-scale equations ([32, 33]), but they are typically derived independently. There are multiple approaches to "upscale" the pore-scale solutions to understand the meaning of parameters derived initially at the porous media scale. The upscaling from Navier-Stokes to Darcy's Law is one step that is relatively well known (e.g., [52], [74]), the upscaling from pore to porous media scale for the electrokinetic problem is less well developed [23, 66, 5, 72].

The following sections introduce the pore-scale governing equations (Section 2) and the porous media scale governing equations (Section 3). One accepted journal publication has already been completed from this project on the topic of uncoupling the porous media scale governing equations [42], which is introduced in Section 3.2. The academic alliance portion of the LDRD has produced one journal paper, which is in review on the topic of pore-scale numerical modeling the effects of tortuosity (Section 4.1), while the manuscript on using machine learning to upscale

pore-scale flow to porous media scale is approaching submission (Section 4.2). A laboratory effort to measure streaming potential and electroosmotic coupling coefficents in 823/B59 is outlined in Section 5.

2. PORE-SCALE EQUATIONS

Predicting the pore-scale electrokinetic problem requires simultaneously solving three or more governing equations: Stokes for incompressible, creeping fluid flow, the Nernst-Planck equation for each species in ion transport, and a Poisson equation for excess charge redistribution [61, 18, 51, 41]. These governing equations are already simplifications (e.g., Stokes is simplified from Navier-Stokes for creeping flow; Nernst-Planck is simplified from Stefan-Maxwell for dilute concentrations; Poisson excess charge distribution simplified from Maxwell equations without magnetic effects), but are generally found to be sufficient for relevant pore-scale problems [51].

Fluid flow most generally is governed by the Navier-Stokes equations, but fluid compressibility, non-linear acceleration, and gravity terms are often considered insignificant at small scales. The Nernst-Planck equation assumes the distribution of ions can be treated as a continuum problem governed by electrostatics; a smaller-scale density functional theory, Monte Carlo, or molecular dynamics simulation would need to be used to resolve ion size (i.e., steric) effects or other ionic-strength dependent forces between ions. By solving the electrostatic Poisson equation, we assume there is no significant magnetic field generated (even when applying low-frequency alternating current), and we assume the transient effects of polarization are minimal. The Maxwell equations would need to be solved in a more rigorous formulation that included magnetic field effects due to time-variable charges. Coupling the Navier-Stokes and Maxwell equations with a representation of individual ions would be quite computationally intensive, and is not done here.

2.1. Pore-Scale Fluid Flow (Stokes)

Generally, the Navier-Stokes equations (momentum and mass continuity) for a Newtonian fluid subject to gravitational and electrical body forces are [27]

$$\begin{aligned} \frac{\partial(\rho\mathbf{u})}{\partial t} + \nabla\cdot(\rho\mathbf{u}\mathbf{u}) &= -\nabla p + \nabla\cdot\mu\left(\nabla\mathbf{u} + \nabla\mathbf{u}^T\right) + \rho\mathbf{g} - \rho_f\nabla\psi \\ \frac{\partial\rho}{\partial t} + \nabla\cdot(\rho\mathbf{u}) &= 0 \end{aligned} \tag{2.1}$$

where ρ is fluid density [kg/m^3], $\mathbf{u}$ is the fluid velocity vector [m/s], p is fluid pressure [Pa], μ is dynamic viscosity [Pa·s], $\mathbf{g} = -g\hat{\mathrm{k}}$ is the gravitational acceleration vector [m/s^2], ρ_f is the free charge density [C/m^3] (as opposed to bound charge from polarization), and ψ is the electrostatic potential [V].

The last source term in the Navier-Stokes equation accounts for electroosmosis. At the pore scale, the characteristic lengths are very small, such that the Reynolds numbers are small for liquids

except for large velocities. The gravity term in the Navier-Stokes is typically unimportant in pore-scale problems; it is often set to zero. For incompressible (constant ρ) flow at low Reynolds number, both equations can be significantly simplified (but the non-linear diffusion terms can sometimes make the Navier-Stokes equations easier to solve than the stiffer Stokes equations). These simplifications lead to the transient Stokes flow problem:

$$\begin{aligned} \rho \frac{\partial \mathbf{u}}{\partial t} &= -\nabla p + \nabla \cdot \mu \nabla \mathbf{u} - \rho_f \nabla \psi \\ \nabla \cdot \mathbf{u} &= 0. \end{aligned} \tag{2.2}$$

The first equation is momentum conservation in creeping flow, and the second equation is the revised mass continutity equation, which now simply requires the velocity field to be solenoidal (divergence-free).

Even with these simplifications, solutions for linear transient Stokes flow are typically performed numerically; it is a set of 4 equations in 4 unknowns (3 components of $\mathbf{u}$ and p). It is possible to solve (2.2) using finite volume ([55], [27], or FiPy) or finite element (e.g., Elmer, SfePy, deal.II, or FEniCS).

When solving the stokes problem numerically, often the continuity equation is used to adjust the pressure, by solving a Poisson-type equation that ensures the solution is divergence-free. The SIMPLE scheme is summarized by as (e.g., [55], [27]):

- start with guess of pressure and velocity fields ($\mathbf{u}$ is assumed to be divergence free);
- compute the viscous term, the source term;
- solve a Poisson equation for pressure, using the previous terms as the inhomogeneous terms;
- compute the velocity field at the next time step (it will be divergence free); and
- advance to the next time step.

Despite being a significant simplification from the Navier-Stokes equations, Stokes flow is still non-trivial to solve, because there is not an equation to derive the pressure field from, and this is typically not known *a priori*. There are several common solution strategies for the Stokes equations, including modifying them to create a pressure equation that simultaneously leads to a solenoidal velocity field and therefore satisfies the mass continuity equation.

2.2. Dilute Pore-Scale Ion Transport (Nernst-Planck)

Transport of dilute concentrations of ions in an electrolyte at the mesoscale is governed by the Nernst-Planck equation [61, 51]. Direct molecular dynamics simulation of individual molecules of water and solute represents smaller time and length scales (e.g., like LAMMPS). Some of the limitations of this representation include ([18, §4.3], [38]):

- Finite size of ions is neglected (i.e., close to solid surface, ion concentration can be very high);

- Finite size of ion hydration spheres;
- Ignore discrete nature of ions (i.e., they are actually multiples of the fundamental charge);
- Ignore finite nature of surface charge;
- Ignore non-Coulombic interaction (i.e., not including effects of water hydration shells or ion dipoles);
- Ignore variations in water permittivity near solid surface;
- Surfaces are assumed to be locally flat; and
- Solution is derived in dilute limit (i.e., no multiple-ion interactions like Pitzer).

The Nernst-Planck expression for the total ion flux of the ith dilute species is [61, 24]

$$\mathbf{j}_i^{**} = \underbrace{n_i \mathbf{u}}_{\text{convection}} \underbrace{- D_i \nabla n_i}_{\text{diffusion}} \underbrace{- n_i \frac{z_i e D_i}{k_B T} \nabla \psi}_{\text{migration}}, \tag{2.3}$$

where n_i is the number concentration $[1/\mathrm{m}^3]$ for the ith species, D_i is the diffusion coefficient $[\mathrm{m}^2/\mathrm{s}]$ for the ith species in the solvent (i.e., water), z_i is the dimensionless integer ion valence, e is the fundamental electron charge $[1.602 \times 10^{-19}\ \mathrm{C}]$, k_B is the Boltzmann constant $[1.381 \times 10^{-23}\ \mathrm{J/K}]$, and T is absolute temperature [K]. The mass concentration c_i of the ith species $[\mathrm{kg/m}^3]$ and number concentration are related through the molecular weight M_i [kg] for a given species

$$c_i = M_i n_i. \tag{2.4}$$

The coefficient in the last term of (2.3) can be written equivalently as $\frac{z_i \mathscr{F} D_i}{RT}$, where $\mathscr{F} = eN_A$ is the Faraday constant $[9.649 \times 10^4\ \mathrm{C/mol}]$, R is the universal gas constant $[8.314\ \mathrm{J/(mol{\cdot}K)}]$, and N_A is the Avagadro constant $[6.022 \times 10^{23}\ 1/\mathrm{mol}]$.

The current density vector, $\mathbf{i}$ $[\mathrm{A/m}^2]$, can be related to the sum of the fluxes of all N charged species

$$\mathbf{i} = e\mathbf{u} \sum_i^N z_i n_i - e \sum D_i^N z_i \nabla n_i - \frac{e^2}{k_B T} \nabla \psi \sum_i^N z_i^2 D_i n_i \tag{2.5}$$

by summing over all the ions and multiplying by the appropriate constant. The coefficient in the third term (i.e., migration) of (2.5) is bulk electrolyte electrical conductivity $[\mathrm{S/m}]$

$$\sigma_0 = \frac{\mathscr{F}^2}{RT} \sum z_i^2 D_i c_i = \frac{e^2}{k_B T} \sum z_i^2 D_i n_i. \tag{2.6}$$

This shows the local electrical conductivity depends on concentration and the diffusion coefficient, which also may be a function of concentration.

The electrostatic charge conservation equations for individual species are

$$\frac{\partial n_i}{\partial t} = -\nabla \cdot \mathbf{j}_i^{**}, \tag{2.7}$$

and the familiar total current density conservation equation is obtained by again summing over all N charged species

$$e\sum_{i}^{N} z_i \frac{\partial n_i}{\partial t} = \frac{\partial \rho_f}{\partial t} = -\nabla \cdot \mathbf{i}, \tag{2.8}$$

where the definition of excess charge distribution $\left(\rho_f = e\sum_i z_i n_i\right)$ is used.

For electrically neutral solutions, $\rho_f = 0$ over typical macroscopic volumes (i.e., many pores). If an electrolyte consists only of water and equal concentrations of ions derived from a common solute (e.g., Na^+ and Cl^- from salt), then $\sum_i z_i n_i = z_+ n_+ + z_- n_- = zn - zn = 0$ ($z_+ = -z_- = z$ and $n_+ = n_-$ for a 1:1 electrolyte). For water far from container/pore walls, the electroneutrality condition is satisfied. Near a charged surface (i.e., a pore wall or a central ion [15]), there will be an excess of counterions, which balance the immobile surface charge.

2.3. Pore-Scale Excess Charge Redistribution (Poisson)

In the electrostatic limit (i.e., no magnetic fields), the electric field is governed by

$$\nabla \cdot \mathbf{E} = \frac{\rho_f}{\varepsilon} + \rho_b, \tag{2.9}$$

where ρ_b is the distributed "bound" charge due to polarization effects, $\varepsilon = \varepsilon_0 \varepsilon_r$ is the permittivity of the liquid [F/m or C/(V·m)], ε_0 is the permittivity of free space $[8.854 \times 10^{-12}$ F/m], and $\varepsilon_r \approx 80$ for water at 25° C. Static permittivity (i.e., in the DC limit) of water decreases with increases temperature and salinity; $\varepsilon = \varepsilon(c_i, T)$. Permittivity is also a function of frequency, but is relatively constant at low frequencies considered here ($<$ 1kHz).

Maxwell's equations require $\nabla \times \mathbf{E} = 0$, which can be enforced by equating the electric field to the gradient of a scalar potential, $\mathbf{E} = -\nabla\psi$ (e.g., [7]).

$$\nabla^2 \psi = \frac{\rho_f}{\varepsilon} + \rho_b. \tag{2.10}$$

Equation (2.10) is a steady-state distribution of scalar electrostatic potential, with the bound polarization charge and excess charge distribution acting as a source terms.

These equations are solved numerically using OpenFOAM [39] in the two applications discussed in Section 4. We now move up to the porous media (i.e., macroscopic) scale, where the individual pores are not resolved, but treated with a new set of equations.

3. POROUS MEDIA SCALE EQUATIONS

3.1. Streaming Potential and Electroosmosis

The macroscopic (i.e., porous media) scale electrokinetic problem requires simultaneously solving two governing equations: the transient groundwater flow equation (i.e., diffusion) and a Poisson equation for excess charge redistribution. We develop expressions for the Darcy and electric current densities (i.e., fluxes) simultaneously in terms of potential gradients (i.e., thermodynamic forces)

$$\begin{aligned} \boldsymbol{j}_e &= -\sigma_0 \nabla \psi - L_{12} \nabla p \\ \boldsymbol{j}_f &= -L_{21} \nabla \psi - \frac{k_0}{\mu} \nabla p \end{aligned} \tag{3.1}$$

where $\boldsymbol{j}_e$ and $\boldsymbol{j}_f$ are electrical $[\mathrm{A/m^2}]$ and Darcy (i.e., fluid-volume) $[\mathrm{m/s}]$ current densities, k_0 is porous media intrinsic permeability $[\mathrm{m^2}]$, $\{L_{12}, L_{21}\}$ are porous media electrokinetic coupling coefficients $\{[\mathrm{A/(m \cdot Pa)} \rightarrow \mathrm{A \cdot s^2/kg}], [\mathrm{m^2/(V \cdot s)} \rightarrow \mathrm{A \cdot s^2/kg}]\}$[1], ψ is electrostatic potential $[\mathrm{V}]$ (in the quasi-static limit with no magnetic sources), and p is liquid pressure $[\mathrm{Pa}]$. Both p and ψ are changes from an arbitrary initial state due to some forcing (e.g., pumping or recharge), which is conveniently set to zero here. The zero subscripts on k and σ differentiate them from similar quantities (i.e., $\boldsymbol{j}_{\mathrm{Darcy}} = -k/\mu \nabla p$ or $\boldsymbol{j}_{\mathrm{Ohm}} = -\sigma \nabla \psi$) that do not consider electrokinetic coupling effects [58].

The streaming potential coupling coefficient can be given in terms of pore-scale electrokinetic quantities [65, 16] as

$$L_{12} = \frac{\varepsilon \zeta \sigma_0}{\mu \left(\sigma_f + F \sigma_s\right)} \tag{3.2}$$

where ε is the pore-fluid dielectric constant $[\mathrm{F/m}]$, ζ is the zeta potential at the pore/fluid interface $[\mathrm{V}]$, σ_f and σ_s are the electrical conductivity of the individual fluid and solid components, and F is the dimensionless formation factor, defined as the resistivity of the fluid-saturated rock normalized by the pore fluid resistivity. In the geotechnical literature, L_{21} is electroosmotic permeability (k_e) [20, 8], given in similar form as

$$L_{21} = \frac{n \zeta \varepsilon}{4 \pi \mu}, \tag{3.3}$$

where n is dimensionless porosity.

Based on a thermodynamic argument of microscopic reversibility, [53, 54] showed the off-diagonal coupling coefficients in (3.1) are symmetric $(L_{12} = L_{21})$ when the fluxes and forces

[1] expressing the two coupling coefficients in their base SI units shows they are equivalent

are written correctly [47, 22]. Using this equality, these two expressions from different literature (3.2 and 3.3) lead to the equivalence $n = 4\pi\sigma_0/(\sigma_f + F\sigma_s)$. Both expressions may have utility, since in some situations porosity may be known, and the various conductances may not, or vice versa.

Mass and charge conservation expressions are conveniently and symmetrically written in terms of flux divergence as

$$\begin{aligned} -\nabla \cdot \boldsymbol{j}_e &= C^* \frac{\partial \psi}{\partial t} \\ -\nabla \cdot \boldsymbol{j}_f &= nc \frac{\partial p}{\partial t}, \end{aligned} \tag{3.4}$$

where c is compressibility $[1/\mathrm{Pa}]$, and C^* is specific capacitance $[\mathrm{C}/(\mathrm{m}^3 \cdot \mathrm{V})]$, that is the electrolyte charge flowing into a unit volume per unit change in potential [22]. Typically, in streaming potential problems $\nabla \cdot \boldsymbol{j}_e = 0$ [65], but without loss of generality we include a small transient capacitance term to maintain symmetry in the governing equations required by the uncoupling approach.

Substituting the fluxes (3.1) into the conservation equations (3.4) leads to two coupled differential equations in terms of potentials,

$$\begin{aligned} C^* \frac{\partial \psi}{\partial t} &= \nabla \cdot (\sigma_0 \nabla \psi) + \nabla \cdot (L_{12} \nabla p) \\ nc \frac{\partial p}{\partial t} &= \nabla \cdot (L_{21} \nabla \psi) + \nabla \cdot \left(\frac{k_0}{\mu} \nabla p \right). \end{aligned} \tag{3.5}$$

These coupled equations can be written as a matrix differential equation. In the derivation we assume σ_0, k_0, μ, L_{12}, and L_{21} are piecewise constant in space (allowing them to be taken outside the divergence operator), which results in the form

$$\begin{bmatrix} C^* & 0 \\ 0 & nc \end{bmatrix} \frac{\partial}{\partial t} \begin{bmatrix} \psi \\ p \end{bmatrix} = \begin{bmatrix} \sigma_0 & L_{12} \\ L_{21} & \frac{k_0}{\mu} \end{bmatrix} \nabla^2 \begin{bmatrix} \psi \\ p \end{bmatrix}. \tag{3.6}$$

Because of the assumption of piecewise constancy in material parameters which can violate flux continuity at property discontinuities in numerical models with linear interpolation functions, but still allows either layers or regions of different material properties.

This can be additionally re-arranged, multiplying by the diagonal storage properties matrix inverse, leaving

$$\frac{\partial \boldsymbol{d}}{\partial t} = \begin{bmatrix} \alpha_E & \alpha_E K_S \\ \alpha_H K_E & \alpha_H \end{bmatrix} \nabla^2 \boldsymbol{d}, \tag{3.7}$$

where $\boldsymbol{d} = [\psi, p]^T$ is the physical potential vector, $\alpha_H = k_0/(\mu nc)$ is the hydraulic diffusivity $[\mathrm{m}^2/\mathrm{s}]$, $\alpha_E = \sigma_0/C^*$ is the electrostatic potential diffusivity $[\mathrm{m}^2/\mathrm{s}]$, $K_S = L_{12}/\sigma_0$ is the streaming potential $[\mathrm{V}/\mathrm{Pa}]$, and $K_E = L_{21}\mu/k_0$ is the electroosmosis pressure $[\mathrm{Pa}/\mathrm{V} \rightarrow \mathrm{A} \cdot \mathrm{s}/\mathrm{m}^3]$[2].

[2] electroosmotic pressure units (when expressed in SI base units) are equivalent to volumetric charge density, $[\mathrm{C}/\mathrm{m}^3]$

Using this equality, we express porous media permeability in terms of the streaming potential and the electroosmotic pressure ([58, 57]) $K_E = K_S \sigma_0 \mu / k_0$ or

$$k_0 = \sigma_0 \mu \frac{K_S}{K_E}. \tag{3.8}$$

When $L_{12} = L_{21} = 0$ the streaming potential and electroosmotic pressure cease to exist; zeroing these coefficients makes the matrix in (3.7) diagonal, where the flow and electrostatic problems are independent and uncoupled.

Starting with (3.7), we multiply the ψ equation by $L_c^2/(\alpha_H \Psi_c)$ and multiply the p equation by $L_c^2/(\alpha_H P_c)$. Characteristic electrostatic potential ($\Psi_c = P_c K_S$), pressure (P_c), time ($T_c = L_c^2/\alpha_H$), and length (L_c) are used to re-write the equations in non-dimensional form in terms of $x_D = x/L_c$, $t_D = t/T_c$, $p_D = p/P_c$, $\psi_D = \psi/\Psi_c$, and ∇_D^2 (the dimensionless Laplacian). The governing equation becomes

$$\frac{\partial \boldsymbol{d}_D}{\partial t} = \boldsymbol{A} \nabla_D^2 \boldsymbol{d}_D \tag{3.9}$$

where $\boldsymbol{A} = \begin{bmatrix} \alpha_D & \alpha_D \\ aK_D & 1 \end{bmatrix}$ is the dimensionless matrix of Laplacian operator coefficients, $\alpha_D = \alpha_E/\alpha_H$ is the dimensionless electrical/hydrological diffusivity ratio, $\boldsymbol{d}_D = [\psi/\Psi_c, p/P_c]^T$ is the dimensionless potential vector, and $K_D = K_E K_S$ is the dimensionless product of the electroosmotic pressure and streaming potential, representing the magnitude of electrokinetic coupling.

In the formulation presented here these two dimensionless quantities completely characterize the electrokinetic problem, reducing the problem from four free parameters (α_H, α_E, K_S, K_E) to two. This reduction in free parameters does not limit the range of validity of the solution, it properly simplifies the previously over-constrained solution space (two equations in terms of two potentials were related with four parameters). L_c and P_c are chosen from the physical problem configuration (e.g., domain size and applied boundary or initial conditions), while T_c and Ψ_c are specified as part of re-writing the governing equations in dimensionless form.

3.2. Eigenvalue Uncoupling

In a recently accepted journal manuscript [42], we present an eigenvalue uncoupling approach that relies on decomposing the matrix characterizing the operator in the governing equation into a diagonal matrix using its eigenvalues and eigenvectors (i.e., spectral decomposition). The process results in two uncoupled diffusion equations in terms of "intermediate" material parameters and boundary conditions. The simpler and uncoupled intermediate problems are solved with traditional methods, then the fully-coupled solution is found through a matrix multiplication of the intermediate results with a matrix comprised of the eigenvectors of the original problem. While the approach has been used in geophysics to decouple poroelastic wave equations [46], and in quantum mechanics to uncouple second-order differential equations regarding elastic scattering [71, 44], it has not previously been applied to uncoupling electrokinetic processes.

In the recent manuscript [42], we illustrate the process of uncoupling through two examples: the streaming potential response to 1D cylindrically symmetric flow to a confined pumping well (i.e., the Theis solution) and solution for an oscillatory streaming potential and electroosmotic laboratory device.

4. ACADEMIC ALLIANCE: PORE-SCALE NUMERICAL MODELING

During the second and third years of the three-year LDRD project (FY19 and FY20), the authors participated in a partnership funded by the Sandia LDRD Academic Alliance program. Professor Narayana Aluru and postdoctoral researcher Pikee Priya from the Beckman Institute at the University of Illinois at Urbana-Champaign performed pore-scale modeling. The following two sections summarize some of the work done as part of this partnership. Section 4.1 is based on a submitted manuscript to *Transport in Porous Media* (i.e., work is currently under journal peer review), while the Section 4.2 is based on a draft manuscript "Upscaling Electrokinetics via Machine Learning" currently under preparation for submittal to journal peer review.

4.1. Investigating Tortuosity and Electrokinetics

Pore-scale finite-volume continuum models of electrokinetic processes are used to predict the velocity and potential profiles for two-dimensional arrays of circles, ellipses and squares with different orientations. The pore-scale continuum model solves the coupled Navier-Stokes, Poisson, and Nernst-Planck equations to characterize the electro-osmotic pressure and streaming potentials developed on the application of an external voltage and pressure difference respectively (see equations in Section 2). This model is used to predict the macroscale permeabilities of geomaterials (see relationships in Section 3) via the widely used Carman-Kozeny equation [19] and through the electrokinetic coupling coefficients [58, 57]. The effect of the particle aspect ratio and orientation on the electrokinetic coupling coefficients and subsequently the electrical and hydraulic tortuosity of the porous media has been determined. These calculations suggest a highly tortuous geomaterial can be efficient for applications like decontamination and desalination.

A pore-scale continuum model is used to simulate the Electric Double Layer (EDL) in porous materials and the effect of applied pressure/voltage on the fluid flow and current density. However, real-world geomaterials are heterogeneous and complex and it is difficult to understand the individual effects of pore orientation, grain aspect ratios, and overall tortuosity on the observed bulk electrokinetic effect. We, therefore, characterized these effects in regular 2D geometries (circles, ellipses with different aspect ratios, and squares) and determine the electroosmotic pressure, K_E, and streaming potential, K_S, using pore-scale models. Although previous Navier-Stokes simulations have been performed to confirm relationships between permeabilities, pore particle geometries, porosities, and tortuosities [76], benchmarking of electrokinetics through the quantitative pore-scale determination of K_E and K_S has not yet been performed. Here, we predict the effect of hydraulic and electrical tortuosities on electrokinetics in these geometries.

4.1.1. Numerical Model

A pore-scale continuum finite volume model implemented in OpenFOAM [39] has been used for the characterization of electroosmosis (EO) and streaming potential (SP) in geomaterials and regular geometries. An iterative implementation of the SIMPLE algorithm (Section 2.1) is used to solve the Navier-Stokes equations at each step, coupled with the Nernst-Planck (Section 2.2) and Poisson (Section 2.3) equations. The segmented binary microstructural images of the geomaterials are converted into stereolithiography (STL) files using DREAM3D [34]. These STL files are then imported into Gmsh [28] to create the solution mesh. The initial Gmsh mesh is imported into OpenFOAM and subsequently refined near the charged pore surfaces to capture the ion accumulation in the EDL 'diffuse' layer for very dilute NaCl solutions (0.05 $\mathrm{mol}/\mathrm{m}^3$).

The pore-scale governing equations are solved on a two-dimensional mesh of prismatic control volumes representing the pore space in a porous material (i.e., the grains are assumed impenetrable by the fluid phase and resistive enough to not contribute to bulk electrical conduction). The approximate domain size is 5 μm with control volume in the range of 4 to 10 nm with the smaller control volumes near the pore surfaces. The number of finite volume elements in any simulation are in the range 100,000 to 300,000. A constant-pressure difference (for SP characterization) and constant-potential difference (for EO characterization) are applied across the domain (i.e., between inlet and outlet patches). A no-gradient ($\nabla u = 0$) velocity boundary condition (BC) is applied at the left and right (inlet and outlet) boundaries while a no-slip velocity BC (u=0) is applied at the top and bottom walls. No-gradient electric potential ($\nabla \psi = 0$) and pressure ($\nabla p = 0$) BCs are applied at the top and bottom walls. A constant electrostatic potential equal to the zeta potential [V] is applied at the internal boundaries (i.e., solid-liquid interfaces) for electro-osmotic flow calculations while a constant surface charge density [C/m^2] is applied for the streaming potential calculations. Internal walls have no-slip velocity and no-gradient pressure BCs. An initial condition of a constant concentration of the electrolyte is used.

The EO and SP coefficients, K_E and K_S, and associated permeability k_0, were calculated from porous media scale relationships (Section 3.1). These permeabilities were compared to the Carman-Kozeny (CK) relationship [19] and the Schwartz-Sen-Johnson model [68, 43].

4.1.2. Results

Pengra et al. (1999) [58, 57] presented the macro-scale relationship between permeability and electrokinetics coupling coefficients in porous materials (Section 3.1). Permeabilities estimated from electrokinetic coupling are compared to the permeabilities predicted only by geometry using the CK relation. These two estimates are reconciled through the hydraulic tortuosity for the regular geometries.

A summary of the dependence of K_E and K_S (estimated from model results) on τ_h and τ_e (estimated from the CK and SSJ models) is shown in Figure 4-1, respectively. Both K_E and K_S seem to depend more-or-less linearly on τ_h, with τ_d remaining near unity for all the geometries. Differences between geometric or hydraulic and electrical tortuosities are well-known [29]. The

maximum K_E value corresponds to $\tau_h = 30$ for ellipses oriented at 60° with $c/a = 2$ and the maximum K_S value is for ellipses oriented at 90° with $c/a = 3$. The maximum tortuosity of about 43 is obtained for ellipses oriented at 30° with $c/a = 2$. This implies that for a highly tortuous porous material (i.e., more pore bodies, more mixing of flowpaths, and shorter pore throats), the diffuse ions will move upon application of an electric potential difference, mobilizing the bulk fluid. However, a direct-current driving potential cannot be increased over the dielectric breakdown limit. Also, when applying pressure gradient across a highly tortuous material, the fluid moves, but with less net transport of charges. This could be exploited in applications like desalination or decontamination using highly tortuous geomaterials. At the other end lies materials with very low aspect ratio ($\rightarrow 0$) and low tortousity ($\rightarrow 1$), as is the case of pores in regularly packed materials. The K_E and K_S values increase with electric tortuosity (Figure 4-1).

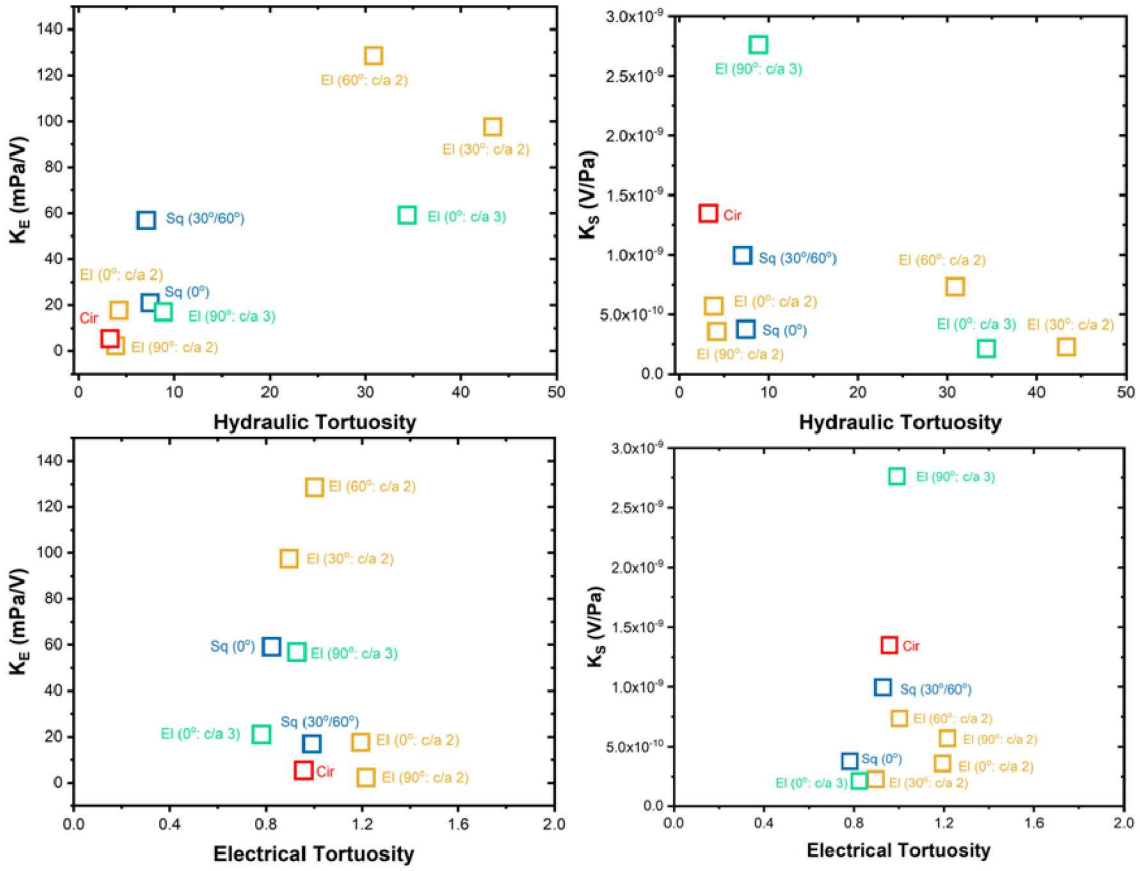

Figure 4-1. The effect of hydraulic (τ_h) and electrical (τ_e) tortuosities on electroosmosis (K_E) and streaming potential (K_S) coupling coefficient values for arrays of regular 2D bodies.

4.1.3. Conclusions

This section illustrated application of a finite-volume continuum model to solve coupled pore-scale electrokinetics and fluid flow equations, to predict the EO pressures arising from applied voltage and SP potentials arising from applied pressure differences, in two-dimensional

domains comprising arrays of circles, ellipses and squares of various orientations to better understand tortuosity and path complexity effects on geomaterials. To understand electrokinetics in geomaterials, flow through different regular geometries of pores of comparable sizes are characterized. This is one of the first works on benchmarking electrokinetics in arrays of regular geometries. The calculated hydraulic tortuosities suggest highly tortuous geomaterials can be very effective in applications like desalination and decontamination.

4.2. Investigating Machine Learning to Upscale Fracture Networks

Extending the modeling presented in the previous section, and building on Bernabe's early work on flow and electrokinetics in networks of cracks and pores [11, 12], we are working to upscale electrokinetic flow through a network of intersecting fractures. The goal of this work is to predict the macroscopic streaming potential and electroosmosis behavior of the system, by training the network with pore-scale simulations. Then given a pore-scale fracture network, the macroscopic behavior could be predicted. Historically, flow and transport were solved through a finite networks of random intersecting fractures as a matrix problem [3, 13, 67].

A series of sparsely-fractured synthetic 2D domains were created (Figure 4-2), and the pore-scale equations (Section 2) were solved using the OpenFOAM numerical modeling framework discussed in Section 4.1.

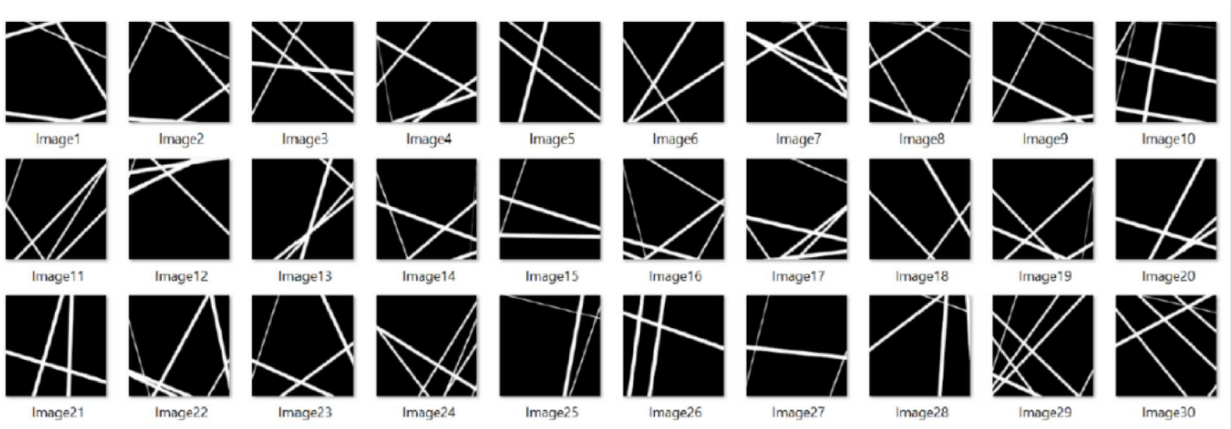

Figure 4-2. Sparsely-fractured 2D domains for training machine learning

The SP and EO electrokinetics problems were numerically simulated on these 2D domains at 4 different orientations (left to right, right to left, top to bottom, and bottom to top) to gather data for training the machine learning algorithms. The state variables of the problem (fluid pressure, potential, and fluid velocity) were sampled from the solution mesh at pore cross sections and intersections, along with statistics about the geometry (pore diameter, pore length between intersections, angle made between pores at intersection) to build a training dataset (Figure 4-3) for machine learning.

From 15,000 to 25,000 data points were used to train network architectures with different numbers of hidden layers. Figure 4-4 shows the improvement in error through training for each

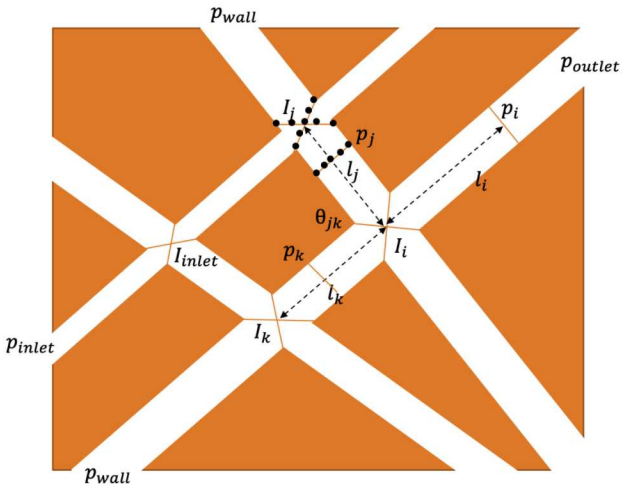

Figure 4-3. Example of sample locations (dots) at a typical intersection of 2D fractures (white gaps between orange blocks)

network (green box indicates best network for each case). For flow from the wall to the first intersection, a system with 8 hidden layers performed best, while for the flow from the next intersection to the wall, a smaller network with only 4 hidden layers performed better.

These intermediate results illustrate the framework and data are in place (i.e., coupled pore-scale physics simulations at a high resolution), but some experimentation may be required to arrive at a feasible upscaled prediction. While there is a large improvement in error due to training, the mean absolute error at the end of training was around 5%.

To accurately simulate the results, the machine learning must take into consideration multiple things:

1. The state of the pore-scale electrokinetic solution,
2. The connectivity and geometry of the fracture network, and
3. The boundary conditions (i.e., applied voltage or applied pressure) on the domain.

while making its prediction of overall electrokinetic properties of the network, seeking to arrive at a result similar to Bernabe [12], but using a machine learning approach.

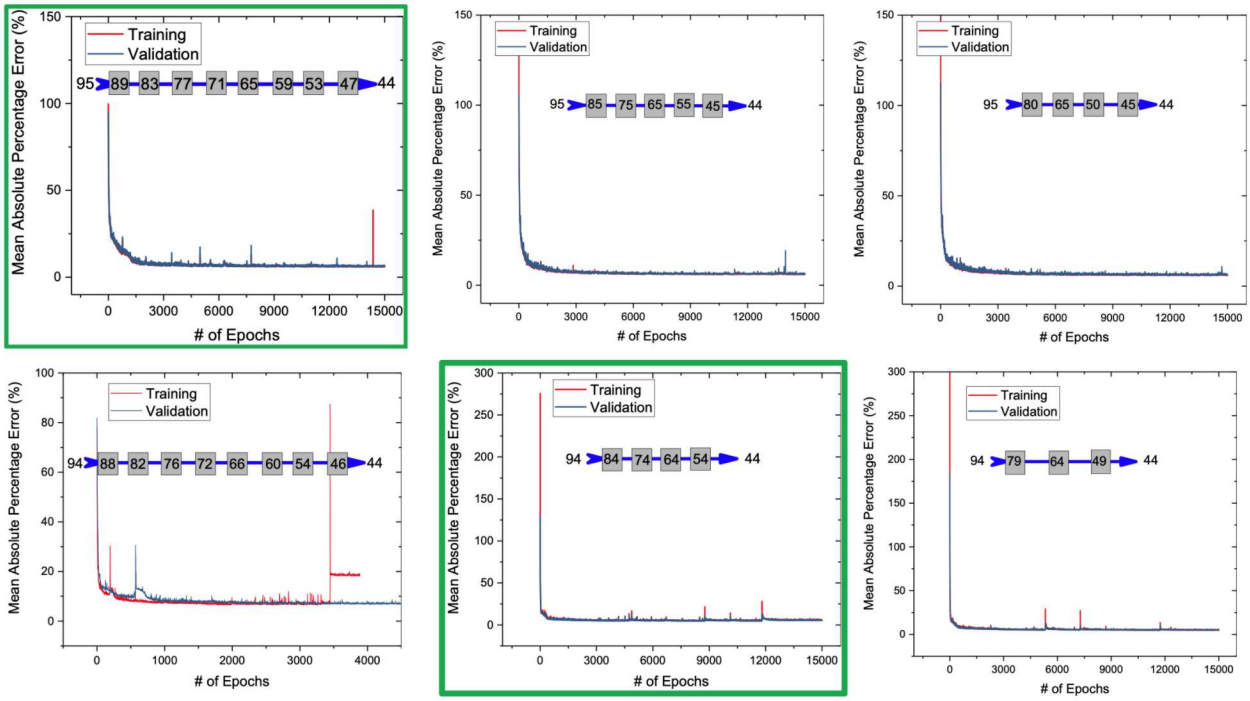

Figure 4-4. Examples of training for flow from wall to first intersection (top) and from intersection to subsequent pore (bottom). Green box indicates best prediction. Chain shows number of layers and number of connections per layer

5. 823 LABORATORY EXPERIMENTS

In the laboratory in B59/823, a progression of laboratory implementations were created to estimate sample permeability through estimates of the streaming potential (K_S) and the electroosmotic pressure (K_E) using a modification of the method described in a paper by Pengra et al. (1999) [58]. The laboratory approach was not ultimately successful in measuring both the streaming potential and the electroosmostic pressure with reasonable accuracy. Other approaches have recently been found that may represent a better approach [30, 31]; however with COVID-19 restrictions and recent construction in the B59 laboratory these approaches could not be pursued.

5.1. Flow-through Streaming Potential Measurements

First, streaming potential was measured in an Ottawa sand column, driven by a Mariotte bottle upstream constant head source, and a variable-position outlet (Figure 5-1).

Figure 5-1. Flow-through streaming potential device

The streaming potential coupling coefficient was estimated to be 0.00358 $\mathrm{V/m\,H_2O}$ (3.65×10^{-7} V/Pa) from the steady-state voltage response at each different applied pressure drop (Figure 5-2). These measurements were successful, and show the streaming potential coefficient

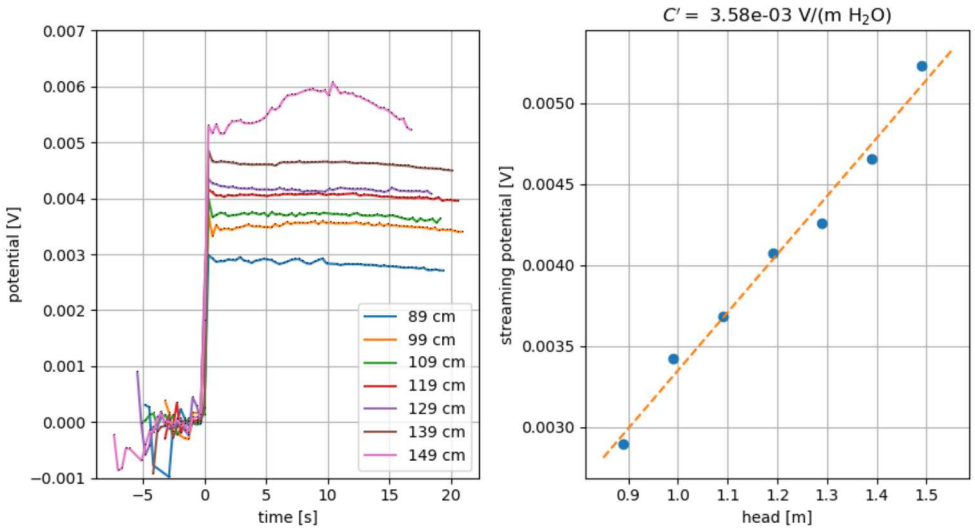

Figure 5-2. Streaming potential response for flow-through device

is relatively straightforward to measure in the laboratory.

5.2. Pengra-Style Laboratory Device

The second device was constructed consisted of two pairs of $Ag/AgCl_2$ biomedical electrodes, a hydrophone, and an Omega differential pressure transducer, similar to the design used by Pengra et al [57, 58]. The Ottawa sand sample was sealed in with epoxied porous end caps within a 1.5-inch diameter clear PVC pipe. The end caps were cut from a 1.5-mm thick Porex polyethylene sheet with a pore size of 50–90 μm. The sample was then flooded slowly with 0.05-M NaCl brine from one side until it was saturated, to minimize trapped air bubbles within the sample.

In this device the plan was to perform two conjugate experiments on the same sample. One experiment would apply a low-frequency pressure pulse to the sample, measuring the resulting low-frequency electrical response (i.e., streaming potential). The second experiment would apply a low-frequency electrical excitation to the sample, measuring the resulting low-frequency pressure response (i.e., electroosmotic pressure).

To improve the sensitivity of the observations, a National Instruments high-frequency (>50 kHz) analog voltage data acquisition system was purchased. Using this system revealed several flaws in the design of the overall electrokinetic apparatus, discussed in the next section.

5.3. Issues with Apparatus

The sealed hydrophone (located inside the longer right side of the device – Figure 5-4) did not create enough pressure signal to result in a measurable streaming potential signal since the low-voltage requirements in the laboratory required keeping the applied voltage on the

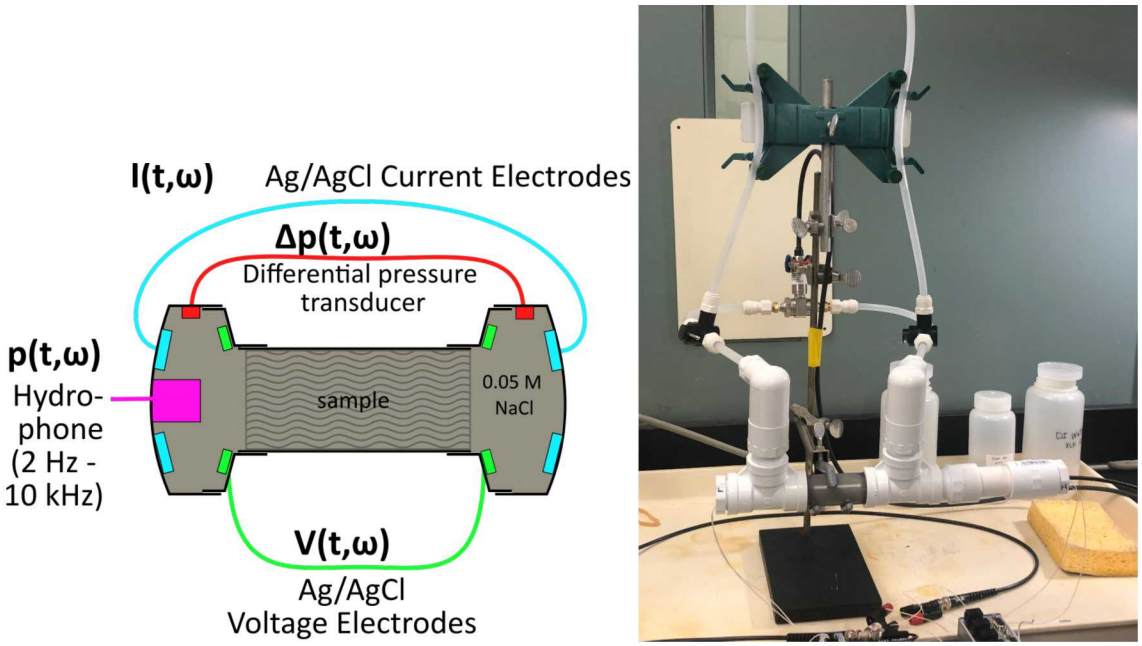

Figure 5-3. Diagram and photograph of laboratory device in 823/B59

hydrophone below 50 V. The hydrophone was driven at approximately 200 Hz; the response of the hydrophone as a function of frequency is illustrated in Figure 5-5. This shows the response predicted is below 100 μPa/V. The result was audible in the laboratory, but the differential pressure measured between the two sides was not enough to drive a streaming potential response observable with the electrodes. A different hydrophone with a stronger low-frequency response, or a physically driven piston or pump (e.g., similar to [31, 30]) would have resulted in a stronger signal. The metal-bodied differential pressure transducer also evidently was electrically part of the circuit, making simultaneous measurement of pressure and application of current impossible. A pair of electrically isolated pressure transducers or a non-conducting differential pressure transducer would be needed to measure pressure signals in the system. The device was constructed from plastic to minimize short circuits in the system, but efforts to electrically isolate the pressure transducer were not successful (using parafilm as a non-conducting membrane to separate the fluids in each part of the apparatus from one another). A differential pressure transducer was chosen to increase sensitivity, but two independent pressure transducers would have improved electrical isolation (at the expense of the error associated with subtracting two similar values). The Omega specification states at least 10-MΩ resistance between the body and any wire, but measuring the resistance between the pressure transducer wires and the $Ag/AgCl_2$ electrodes gave a value much smaller than this ($\approx$ 10 kΩ).

5.4. Experimental Path Forward

Even after a few re-designs and re-builds of the apparatus to improve electrical isolation and sensitivity, there were some problems with the design that require starting over to achieve. Since the beginning of the project, the authors have become aware of work going on by Glover and his

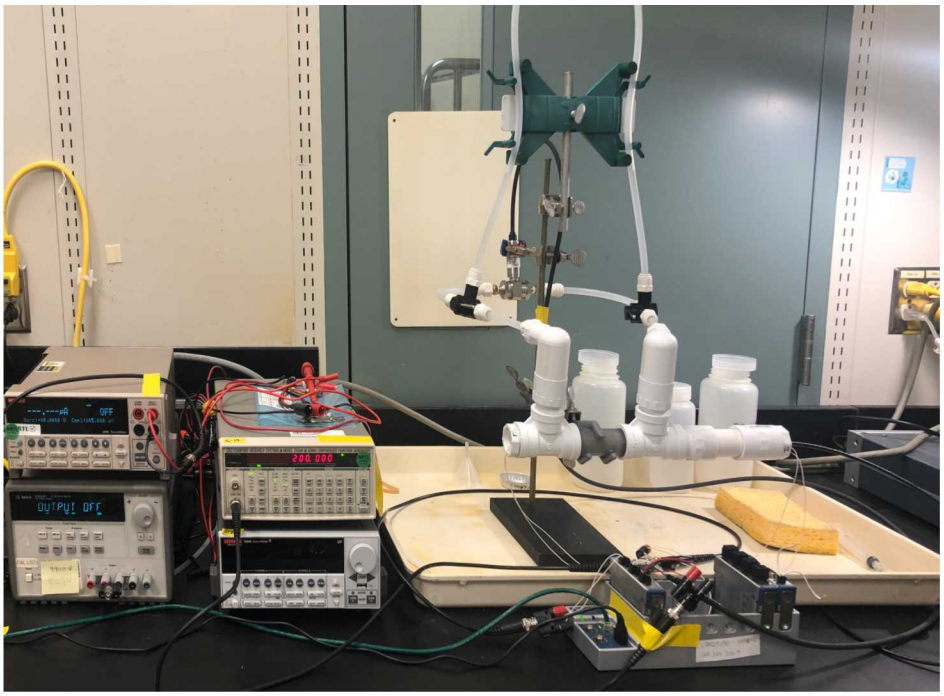

Figure 5-4. Laboratory device above to right with some data acquisition equipment (National Instruments CompactDAQ for high-frequency voltage below, Keithley SourceMeters, DC voltage supply, and function generator to left)

group at University of Leeds to measure periodic streaming potential and electroosmosis coefficients [31, 30, 56]. Some of the recent papers from this group have included designs that may be a better design than the approach of Pengra et al. (1999) [57, 58] chosen here.

For the Ottawa sand used here, using the steady-state coupling coefficient relationship (3.8), the streaming potential coefficient measured in the flow-through apparatus ($K_S = 3.65 \times 10^{-7}$ V/Pa) with the electrical conductivity of 10 mS/cm [75], a viscosity of 8.9×10^{-4} Pa · s and an approximate hydraulic conductivity of 0.01 cm/s [26], we can estimate the expected electroosmotic pressure coefficient. Putting everything into compatible units

$$
\begin{aligned}
k_0 &= \frac{\sigma_0 \mu K_S}{K_E} \\
K_E &= \frac{10^{-2}\,[\mathrm{S/m}] \cdot 10^{-3}\,[\mathrm{Pa \cdot s}] \cdot 10^{-7}\,[\mathrm{V/Pa}]}{10^{-11}\,[\mathrm{m^2}]} \\
K_E &= \frac{10^{-2}\,[\mathrm{s^3 \cdot A^2/(kg \cdot m^2)}] \cdot 10^{-3}\,[\mathrm{kg/(m \cdot s)}] \cdot 10^{-7}\,[\mathrm{m^3/(s \cdot A)}]}{10^{-11}\,[\mathrm{m^2}]} \\
K_E &= 0.1\,[\mathrm{Pa/V}] = 1.5 \times 10^{-5}\,[\mathrm{psi/V}] \qquad (5.1)
\end{aligned}
$$

which agrees to an order-of magnitude with tables reported in [58]. Applying approximately 10 V means an expected signal of 1 Pa or 1/10,000 of a psi. The Omega differential pressure transducer claims it is accurate to 0.4–0.05 % of full range (0.36 psi), which is 1.8×10^{-4} psi (at best). Theoretically, the setup should have been able to detect the coupling coefficient for Ottawa sand,

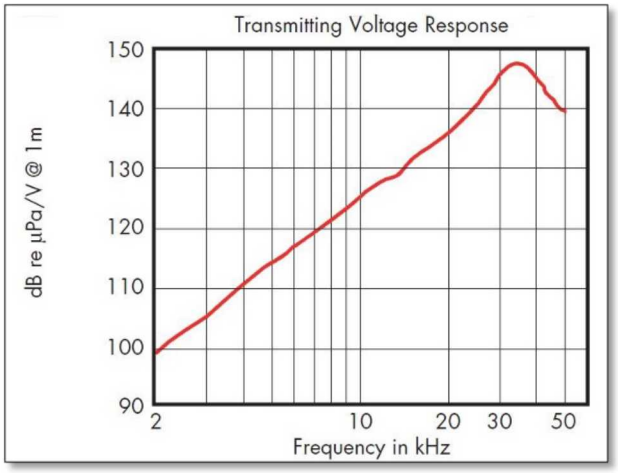

Figure 5-5. Response profile of hydrophone

but it is just on the edge of measurability. Any noise or complicating issues will obscure this, and subtracting two absolute pressures from one another will likely not be as accurate as a differential pressure transducer. To achieve higher electroosmotic pressures would require a much more applied voltage to the $Ag/AgCl_2$ electrodes (which would exceed the 50 V environmental safety and health "low voltage" exemption), saltier, or less viscous fluid. Higher salinity would raise σ_0, but it would lower K_S, so it is difficult to change the resulting K_E value much without making the water much saltier (which complicates the types of materials that can be used).

6. OVERALL CONCLUSIONS

This SAND report summarizes the work done as part of this LDRD to utilize electrokinetics for understanding flow in low-permeability geomaterials. While the laboratory work in 823 was not as successful as hoped, one journal manuscript was published on a novel eigenvalue uncoupling approach for electrokinetic problems, and another journal manuscript with the Academic Alliance is under review. A second academic alliance manuscript is being prepared, and another journal manuscript on transient electrokinetic effects is being prepared. The academic alliance has successfully created a collaboration between Sandia and Professor Aluru and postdoc Priya at Illinois. Once COVID-19 related travel restrictions are lifted, it is planned for Professor Aluru to present a seminar at Sandia, reciprocating the seminar that Kris Kuhlman presented at Illinois in November 2018.

This LDRD has laid the groundwork for future endeavors in this area. Theoretical and laboratory work at Sandia will lead to future applications in any of a range of diverse applications of interest to Sandia National Laboratories and the Department of Energy. The pore-scale modeling by University of Illinois has directly attacked the notoriously difficult problem of bridging the gap between pore and porous media scales in geomaterials.

c	bulk media compressibility	$1/\mathrm{Pa}$
c_i	concentration of ith species	kg/m^3
C^*	specific media capacitance	$\mathrm{C}/(\mathrm{m}^3 \cdot \mathrm{V})$
D_i	free-water diffusion coefficient of ith species	m^2/s
g	gravitational acceleration	m/s^2
$\mathbf{i}$	current density	A/m^2
$\mathbf{j}_e$	current density vector	A/m^2
$\mathbf{j}_f$	Darcy flux vector	m/s
j_i^*	ion concentration flux of ith species	$\mathrm{kg}/(\mathrm{m}^2 \cdot \mathrm{s})$
j_i^{**}	ion number concentration flux of ith species	$1/(\mathrm{m}^2 \cdot \mathrm{s})$
k_0	permeability of porous media	m^2
K_E	electroosmotic pressure	Pa/V
K_S	streaming potential	V/Pa
L_{12}, L_{21}	electrokinetic coupling coefficients	$(\mathrm{A} \cdot \mathrm{s}^2)/\mathrm{kg}$
M_i	atomic mass number of ith species	kg/mol
n	porous media porosity	–
n_i	number concentration of ith species	$1/\mathrm{m}^3$
n_∞	far-field number concentration	$1/\mathrm{m}^3$
p	fluid pressure	Pa
T	temperature	K
$\mathbf{u}$	fluid velocity vector	m/s
z_i	ion valence	–
α_E	electrical diffusivity	m^2/s
α_H	hydraulic diffusivity	m^2/s
ε	permittivity of fluid	F/m
ε_r	relative permittivity of fluid	–
ρ	fluid density	kg/m^3
ρ_f	free charge density	C/m^3
ρ_b	bound charge density	C/m^3
σ_0	bulk electrolyte electrical conductivity	S/m
μ	fluid viscosity	Pa·s
ψ	electrostatic potential	V
ζ	zeta potential: charge at Stern plane	V

Table 6-1. Physical quantities

e	1.602×10^{-19}	fundamental electron charge	C
$\mathscr{F}$	9.649×10^4	Faraday constant	C/mol
k_B	1.381×10^{-23}	Boltzmann constant	J/K
N_A	6.022×10^{23}	Avagadro's number	$1/\mathrm{mol}$
R	8.314	Gas constant	$\mathrm{J}/(\mathrm{K} \cdot \mathrm{mol})$
ε_0	8.854×10^{-12}	permittivity of free space	F/m

Table 6-2. Physical constants

REFERENCES

[1] Yalcin B. Acar and Akram N. Alshawabkeh. Electrokinetic remediation, I: Pilot-scale test with lead-spiked kaolinite. *Journal of Geotechnical Engineering*, 122(3):173–185, 1996.

[2] Yalcin B. Acar, Akram N. Alshawabkey, and Robert J. Gale. Fundamentals of extracting species from soils by electrokinetics. *Waste Management*, 13(2):141–151, 1993.

[3] Pierre M. Adler. *Porous Media: Geometry and Transports*. Butterworth-Heinemann, 1992.

[4] A Soueid Ahmed, A Revil, and L Gross. Multiscale induced polarization tomography in hydrogeophysics: A new approach. *Advances in Water Resources*, 134:103451, 2019.

[5] Grégoire Allaire, Robert Brizzi, Jean-François Dufrêche, Andro Mikelić, and Andrey Piatnitski. Ion transport in porous media: derivation of the macroscopic equations using upscaling and properites of the effective coefficients. *Computational Geosciences*, 17(3):479–495, 2013.

[6] Akram N. Alshawabkeh, Thomas C. Sheahan, and Xingzhi Wu. Coupling of electrochemical and mechanical processes in soils under DC fields. *Mechanics of Materials*, 36(5–6):453–465, 2004.

[7] Rutherford Aris. *Vectors, Tensors, and the Basic Equations of Fluid Mechanics*. Dover Publications, 1989.

[8] M. Arnold. Laboratory determination of the coefficient of electro-osmotic permeability of a soil. *Géotechnique*, 23(4):581–588, 1973.

[9] Sunirmal Banerjee and James K. Mitchell. In-situ volume-change properties by electro-osmosis–theory. *Journal of the Geotechnical Engineering Division*, 106(ASCE15370), 1980.

[10] Sunirmal Banerjee and Vichai Vitayasupakorn. Appraisal of electro-osmotic oedometer tests. *Journal of Geotechnical Engineering*, 110(8):1007–1023, 1984.

[11] Yves Bernabé. The transport properties of networks of cracks and pores. *Journal of Geophysical Research*, 100(B3):4231–4241, 1995.

[12] Yves Bernabé. Streaming potential in heterogeneous networks. *Journal of Geophsyical Research*, 103(B9):20872–20841, 1998.

[13] Yves Bernabé and Céline Bruderer. Effect of variance of pore size distribution on the transport properties of heterogeneous networks. *Journal of Geophysical Ressearch*, 103(B1):513–525, 1998.

[14] Luca Bertolini, Luigi Coppola, Matteo Gastaldi, and Elena Redaelli. Electroosmotic transport in porous construction materials and dehumidification of masonry. *Construction and Building Materials*, 23(1):254–263, 2009.

[15] John O'M. Bockris and Amulya K. N. Reddy. *Modern Electrochemistry*, volume 1. Kluwer, second edition, 1996.

[16] John O'M. Bockris and Amulya K. N. Reddy. *Modern Electrochemistry*, volume 1. Kluwer Academic, second edition, 2002.

[17] Clifford J Bruell, Burton A Segall, and Matthew T Walsh. Electroosomotic removal of gasoline hydrocarbons and TCE from clay. *Journal of Environmental Engineering*, 118(1):68–83, 1992.

[18] Hans-Jürgen Butt, Karlheinz Graf, and Michael Kappl. *Physics and Chemistry of Interfaces*. Wiley-VCH, 2003.

[19] Phillip C Carman. Permeability of saturated sands, soils and clays. *The Journal of Agricultural Science*, 29(2):262–273, 1939.

[20] Ing. L. Casagrande. Electro-osmosis in soils. *Géotechnique*, 1(3):159–177, 1949.

[21] D. Coelho, M. Shapiro, J. F. Thovert, and P. M. Adler. Electroosmotic phenomena in porous media. *Journal of Colloid and Interface Science*, 181(1):169–190, 1996.

[22] M. Yavuz Corapcioglu. Formulation of electro-chemico-osmotic processes in soils. *Transport in Porous Media*, 6(4):435–444, 1991.

[23] J.A. Del Río and S. Whitaker. Electrohydrodynamics in porous media. *Transport in Porous Media*, 44:385–405, 2001.

[24] J.A. Del Río and S. Whitaker. Diffusion of charged species in liquids. *Scientific reports*, 6:35211, 2016.

[25] Francis A. L. Dullien. *Porous Media: Fluid Transport and Pore Structure*. Academic, second edition, 1993.

[26] Mohamed El Ghoraiby, Hanna Park, and Majid T Manzari. Physical and mechanical properties of Ottawa F65 sand. In *Model Tests and Numerical Simulations of Liquefaction and Lateral Spreading*, pages 45–67. Springer, 2020.

[27] Joel H. Ferziger and Milovan Peric. *Computational Methods for Fluid Dynamics*. Springer, third edition, 2002.

[28] Christophe Geuzaine and Jean-François Remacle. Gmsh: A 3-D finite element mesh generator with built-in pre-and post-processing facilities. *International journal for numerical methods in engineering*, 79(11):1309–1331, 2009.

[29] Behzad Ghanbarian, Allen G Hunt, Robert P Ewing, and Muhammad Sahimi. Tortuosity in porous media: a critical review. *Soil science society of America journal*, 77(5):1461–1477, 2013.

[30] P. W. J. Glover, R. Peng, P. Lorinczi, and B. Di. Experimental measurement of frequency-dependent permeability and streaming potential of sandstones. *Transport in Porous Media*, 131(2):333–361, 2020.

[31] P. W. J. Glover, R. Peng, P. Lorinczi, and B. Di. Seismo-electric conversion in sandstones and shales using 2 different experimental approaches, modelling and theory. In *EGU2020*, number Abstract 8454. European Geophysical Union, 2020.

[32] William G. Gray and Cass T. Miller. Thermodynamically constrained averaging theory approach for modeling flow and transport phenomena in porous media systems: 1. motivation an overview. *Advances in Water Resources*, 28(2):161–180, 2005.

[33] William G. Gray and Cass T. Miller. *Introduction to the Thermodynamically Constrained Averaging Theory for Porous Medium Systems*. Springer, 2014.

[34] Michael A Groeber and Michael A Jackson. DREAM 3D: a digital representation environment for the analysis of microstructure in 3D. *Integrating materials and manufacturing innovation*, 3(1):5, 2014.

[35] A. Gupta, D. Coelho, and P. M. Adler. Universal electro-osmosis formulae for porous media. *Journal of Colloid and Interface Science*, 319(2):549–554, 2008.

[36] Seth S Haines and Steven R Pride. Seismoelectric numerical modeling on a grid. *Geophysics*, 71(6):N57–N65, 2006.

[37] David W. Hyndman, Jerry M. Harris, and Steven M. Gorelick. Coupled seismic and tracer test inversion for aquifer property characterization. *Water Resources Research*, 30(7):1965–1977, 1994.

[38] Jacob Israelachvili. *Intermolecular and Surface Forces*. Academic, third edition, 2010.

[39] Hrvoje Jasak, Aleksandar Jemcov, Zeljko Tukovic, et al. OpenFOAM: A C++ library for complex physics simulations. In *International workshop on coupled methods in numerical dynamics*, volume 1000, pages 1–20. IUC Dubrovnik Croatia, 2007.

[40] George Karniadakis, Ali Beskok, and Narayan Aluru. *Microflows and Nanoflows: Fundamentals and Simulation*. Springer, 2005.

[41] Brian J Kirby. *Micro-and Nanoscale Fluid Mechanics: Transport in Microfluidic Devices*. Cambridge University Press, 2010.

[42] Kristopher L. Kuhlman and Bwalya Malama. Uncoupling electrokinetic flow solutions. *Mathematical Geosciences*, (in press), July 2020.

[43] Kristopher L Kuhlman and Edward N Matteo. Porosity and permeability: Literature review and summary. In *Mechanical Behavior of Salt IX Proceedings*, Hannover, Germany, 2018.

[44] John C. Light, Robert B. Walker, Ellen B. Stechel, and Thomas G. Schmalz. *R*-matrix propagation methods in inelastic and reactive collisions. *Computer Physics Communications*, 17(1–2):89–97, 1979.

[45] K. Y. Lo, K. S. Ho, and I. I. Inculet. Field test of electroosmotic strengthening of soft sensitive clay. *Canadian Geotechnical Journal*, 28(1):74–83, 1991.

[46] Wei-Cheng Lo, Garrison Sposito, and Ernest Majer. Analytical decoupling of poroelasticity equations for acoustic-wave propagation and attenuation in a porous medium containing two immiscible fluids. *Journal of Engineering Mathematics*, 64:219–235, 2009.

[47] A. V. Luikov. Systems of differential equations of heat and mass transfer in capillary-porous bodies. *International Journal of Heat and Mass Transfer*, 18(1):1–14, 1975.

[48] Bwalya Malama. Theory of transient streaming potentials in coupled unconfined aquifer-unsaturated zone flow to a well. *Water Resources Research*, 50(4):2921–2945, 2014.

[49] Bwalya Malama, Kristopher L. Kuhlman, and André Revil. Theory of transient streaming potentials associated with axial-symmetric flow in unconfined aquifers. *Geophysical Journal International*, 179(2):990–1003, 2009.

[50] Bwalya Malama, André Revil, and Kristopher L. Kuhlman. A semi-analytic solution for transient streaming potentials associated with confined aquifer pumping tests. *Geophysical Journal International*, 176(3):1007–1016, 2009.

[51] Jacob H. Masliyah and Subir Bhattacharjee. *Electrokinetic and Colloid Transport Phenomena*. John Wiley & Sons, 2006.

[52] Shlomo P. Neuman. Theoretical derivation of Darcy's law. *Acta Mechanica*, 25:153–170, 1977.

[53] Lars Onsager. Reciprocal relations in irreversible processes. I. *Physical Review*, 37(4):405–426, 1931.

[54] Lars Onsager. Reciprocal relations in irreversible processes. II. *Physical Review*, 38(12):2265–2279, 1931.

[55] Suhas V. Patankar. *Numerical Heat Transfer and Fluid Flow*. Hemisphere, 1980.

[56] Rong Peng, Bangrang Di, Paul WJ Glover, Jianxin Wei1, Piroska Lorinczi, Pinbo Ding, Zichun Liu, Yuangui Zhang, and Mansheng Wu. The effect of rock permeability and porosity on seismoelectric conversion: experiment and analytical modelling. *Geophysical Journal International*, 219(1):328–345, 2019.

[57] David B. Pengra and Po-Zen Wong. Low-frequency AC electrokinetics. *Colloids and Surfaces A: Physicochemical and Engineering Aspects*, 159(2–3):283–292, 1999.

[58] David B. Pengra, Sidney Xi Li, and Po-Zen Wong. Determination of rock properties by low-frequency AC electrokinetics. *Journal of Geophysical Research*, 104(B12):29485–29508, 1999.

[59] Davina Pollock and Olaf A. Cirpka. Fully coupled hydrogeophysical inversion of a laboratory salt tracer experiment monitored by electrical resistivity tomography. *Water Resources Research*, 48(1), 2012.

[60] Steve Pride. Governing equations for the coupled electromagnetics and acoustics of porous media. *Physical Review B*, 50(21):15678–15696, 1994.

[61] Ronald F. Probstein. *Physicochemical Hydrodynamics: An Introduction*. John Wiley & Sons, second edition, 1994.

[62] A. Revil. Transport of water and ions in partially water-saturated porous media. part 1. constitutive equations. *Advances in Water Resources*, 103:119–138, 2017.

[63] A Revil, C Gevaudan, N Lu, and A Maineult. Hysteresis of the self-potential response associated with harmonic pumping tests. *Geophysical research letters*, 35(16), 2008.

[64] A. Revil, A. Jarani, P. Sava, and A. Haas. *The Seismoelectric Method*. Wiley Blackwell, 2015.

[65] A. Revil and A. Jardani. *The Self-Potential Method*. Cambridge, 2013.

[66] A. Revil, N. Linde, A. Cerepi, D. Jougnot, S. Matthäi, and S. Finsterle. Electrokinetic coupling in unsaturated porous media. *Journal of Colloid and Interface Science*, 313:315–327, 2007.

[67] Muhammad Sahimi. *Flow and Transport in Porous Media and Fractured Rock: From Classical Methods to Modern Approaches*. Wiley-VCH, second edition, 2011.

[68] Lawrence M Schwartz, Pabitra N Sen, and David Linton Johnson. Influence of rough surfaces on electrolytic conduction in porous media. *Physical Review B*, 40(4):2450, 1989.

[69] Andrew P. Shapiro and Ronald F. Probstein. Removal of contaminants from saturated clay by electroosmosis. *Environmental Science and Technology*, 27(2):283–291, 1993.

[70] A Soueid Ahmed, Abderrahim Jardani, A Revil, and Jean-Paul Dupont. Joint inversion of hydraulic head and self-potential data associated with harmonic pumping tests. *Water Resources Research*, 52(9):6769–6791, 2016.

[71] Ellen B. Stechel, Rober B. Walker, and John C. Light. *R*-matrix solution of coupled equations for inelastic scattering. *Journal of Chemical Physics*, 69(8):3518–3531, 1978.

[72] Luong Duy Thanh, Damien Jougnot, Phan Van Do, Aida Mendieta, Nguyen Xuan Ca, Vu Xuan Hoa, Phan Minh Tan, and Nguyen Thi Hien. Electroosmotic coupling in porous media, a new model based on a fractal upscaling procedure. *Transport in Porous Media*, 134:249–274, 2020.

[73] Jurate Virkutyte, Mika Sillanpää, and Petri Latostenmaa. Electrokinetic soil remediation – critical overview. *Science of The Total Environment*, 289(1):97–121, 2002.

[74] Stephen Whitaker. Flow in porous media I: A theoretical derivation of Darcy's law. *Transport in Porous Media*, 1(1):3–25, 1986.

[75] Chomsin Sulistya Widodo, Herenda Sela, and Didik Rahadi Santosa. The effect of NaCl concentraiton on the ionic NaCl solutions electrical impedance value using electrochemical impedance spectroscopy methods. In *AIP Conference Procedings*, 2018.

[76] K Yazdchi, S Srivastava, and Stefan Luding. Microstructural effects on the permeability of periodic fibrous porous media. *International Journal of Multiphase Flow*, 37(8):956–966, 2011.

DISTRIBUTION

Hardcopy—Internal

Number of Copies	Name	Org.	Mailstop
1	Emily Stein	8844	0747
1	Melissa Mills	8844	0747
1	Tracy Woolever	8162	0750
1	D. Chavez, LDRD Office	1911	0359

Email—Internal (encrypt for OUO)

Name	Org.	Sandia Email Address
Technical Library	01177	libref@sandia.gov

Sandia National Laboratories is a multimission laboratory managed and operated by National Technology & Engineering Solutions of Sandia LLC, a wholly owned subsidiary of Honeywell International Inc., for the U.S. Department of Energy's National Nuclear Security Administration under contract DE-NA0003525.